Journal of Alloys and Compounds 502 (2010) 466–471

Contents lists available at ScienceDirect

Journal of Alloys and Compounds

journal homepage: www.elsevier.com/locate/jallcom

Solid-state synthesis and formation mechanism of barium hexaaluminate from mechanically activated Al_2O_3–$BaCO_3$ powder mixtures

Sri Nugroho [a], Zhong-Chun Chen [a,*], Akira Kawasaki [a], M.O.D. Jarligo [b]

[a] Department of Materials Processing, Graduate School of Engineering, Tohoku University, Sendai 980-8579, Japan
[b] Forschungszentrum Jülich GmbH, Institute of Energy Research (IEF-1), D-52428 Jülich, Germany

ARTICLE INFO

Article history:
Received 18 December 2008
Accepted 29 April 2010
Available online 5 May 2010

Keywords:
Oxide materials
Ba-β-Al_2O_3
High-energy planetary ball milling
Mechanical activation
Solid-state synthesis
X-ray diffraction

ABSTRACT

The synthesis and formation mechanism of barium hexaaluminate compound (Ba-β-Al_2O_3) by solid-state reactions between powdered reactants of alumina (Al_2O_3) and barium carbonate ($BaCO_3$) have been investigated. The processes for synthesizing Ba-β-Al_2O_3 phase include mechanically activated milling of Al_2O_3–$BaCO_3$ powder mixtures and subsequent solid-state reactions at high temperatures. The mechanically activated milling results in a significant decrease in the decomposition temperature of $BaCO_3$, hence promotes its reactions with Al_2O_3. Almost monophasic Ba-β-Al_2O_3 can be synthesized by 9–12 h ball milling, followed by heat treatment at 1500 °C for 2 h. The formation of Ba-β-Al_2O_3 phase includes three stages: (i) decomposition of $BaCO_3$, (ii) formation and growth of spherical $BaO{\cdot}Al_2O_3$ particles, and (iii) reaction between Al_2O_3 and $BaO{\cdot}Al_2O_3$ to form Ba-β-Al_2O_3 with an elongated morphology.

1. Introduction

Barium aluminates have several types of stoichiometric compositions, such as barium monoaluminate ($BaO{\cdot}Al_2O_3$), tri-barium monoaluminate ($3BaO{\cdot}Al_2O_3$), barium tetraluminate ($BaO{\cdot}4Al_2O_3$), and barium hexaaluminate ($BaO{\cdot}6Al_2O_3$) [1]. Of which barium hexaaluminate has attracted much attention in some potential applications including catalytic combustion [2] and gas sensor [3], because of its high chemical, physical, and thermal stability as well as high ionic conductivity and high resistance to sintering and thermal shocks. Besides, barium hexaaluminate can function as a reinforcement for ceramic–matrix composites as reported by Chen et al. [4,5]. The existence of elongated barium hexaaluminate phase with a layered structure is believed to be able to enhance the fracture toughness of Al_2O_3 matrix composites.

In addition to stoichiometric aluminates, barium can form a large number of complex nonstoichiometric Ba–O–Al aluminates. In fact, it is well established that barium hexaaluminate is actually constituted by two distinct phases with defective β-Al_2O_3 structure, *i.e.*, Ba-β_I-Al_2O_3 and Ba-β_{II}-Al_2O_3. β_I with a composition of $Ba_{0.75}Al_{11}O_{17.25}$ (Al/Ba = 14.67) is poorer in barium, while β_{II} with a composition of $Ba_{2.33}Al_{21.33}O_{34.33}$ (Al/Ba = 9.15) is richer in barium [2,6–9]. From Al_2O_3–$BaO{\cdot}Al_2O_3$ phase diagram [6], Ba-β_I-Al_2O_3 has a higher melting point than Ba-β_{II}-Al_2O_3. The present paper is focused on the Ba-β_I-Al_2O_3 phase and it is expressed as Ba-β-Al_2O_3 hereinafter.

There are many methods for synthesizing barium hexaaluminate, such as solid-state reaction [10–12], sol–gel process [13], hydrothermal precipitation [2,14], alkoxide route [10], and spray-inductively coupled plasma techniques [15]. Most of these methods require an additional high-temperature heat treatment before the barium hexaaluminate phase is formed. Solid-state reaction method is still widely used even though it leads to relatively large particle sizes and sometimes particle agglomeration. This method can yield almost monophasic barium hexaaluminate and is suitable for mass production. Different from conventional solid-state reaction techniques, in this research, a high-energy planetary ball-milling method was applied to reduce the particle sizes and enhance the reactivity of constituent powders. The mechanically activated powders possess better sinterability than those synthesized by a conventional solid-state reaction technique [16]. With regard to other methods, such as precipitation–calcination route, a large amount of impurities, *e.g.* alumina, barium carbonate, barium monoaluminate or unknown phase, are usually formed [1,14]. In addition, alkoxide route is of limited industrial interests due to a high cost of alkoxide reagent [17].

So far, some research work [2,9] has concerned with the reaction mechanisms on formation of Ba-β-Al_2O_3 phase. To the knowledge of the present authors, however, the formation mechanism of Ba-β-Al_2O_3 phase has never been reported before from the viewpoint of morphological evolution with varying the temperature. The knowl-

* Corresponding author at: Department of Mechanical and Aerospace Engineering, Graduate School of Engineering, Tottori University, Koyama-minami 4-101, Tottori 680-8552, Japan. Tel.: +81 857 31 5707; fax: +81 857 31 5707.
E-mail address: chen@mech.tottori-u.ac.jp (Z.-C. Chen).

0925-8388/$ – see front matter © 2010 Elsevier B.V. All rights reserved.
doi:10.1016/j.jallcom.2010.04.198

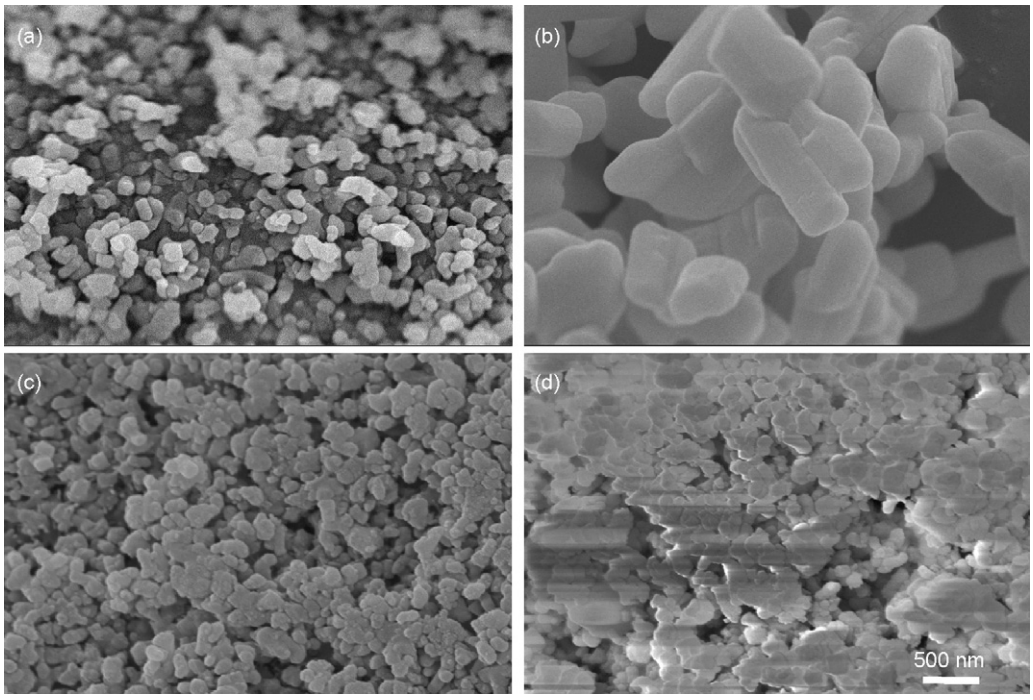

Fig. 1. SEM images of starting powders: (a) alumina, (b) barium carbonate, and powder samples milled for (c) 9 h and (d) 72 h.

edge of the formation mechanism of Ba-β-Al_2O_3 is very helpful to understand the effect of composition and processing parameters on densification behavior, microstructure, and mechanical properties (in particular, fracture strength and fracture toughness) of the related materials. The aims of this work were to synthesize monophasic Ba-β-Al_2O_3 powder through mechanically activated milling and solid-state reaction of alumina and barium carbonate powder mixtures and to get further understanding of its formation mechanism.

2. Experimental procedure

Commercially available α-Al_2O_3 (>99.9% purity, average particle size of 0.17 μm) and $BaCO_3$ (>99.9% purity, average particle size of 1.5 μm) powders were used as the starting materials. Two kinds of powders were mixed with a nominal composition of $Ba_{0.75}Al_{11}O_{17.25}$. The milling operation was carried out in a Fritch Pulverisette type planetary ball-milling system in ethanol at room temperature for 0–72 h. A 250 ml zirconia vial and zirconia balls with a diameter of 5 mm were used as a milling medium. The ball to powder ratio was equal to 10:1. The milling speed was set at 200 rpm. After milling, the slurries were dried at 110 °C for 24 h in an oven. The resultant powder mixtures were heat-treated at 1500 °C for 2 h under air atmosphere. Some powder mixture was heat-treated in a temperature range of 400–1500 °C for 2 h in order to study the formation mechanism of Ba-β-Al_2O_3.

The thermal characteristics of the powder mixtures during reaction were measured by thermogravimetric analysis (TG-DTA 6300, Seiko) and differential scanning calorimetry (DSC 6300, Seiko). In both cases, a platinum crucible was used as a reference and the measurements were conducted in air at a heating rate of 10 °C/min. Powder X-ray diffraction analysis (XRD, Rigaku) was used to determine the crystalline phase in the milled and heat-treated samples. The average crystalline sizes of the milled powders were estimated using the Scherrer formula. The microstructures of heat-treated samples were observed using field-emission scanning electron microscopy (FE-SEM, JEOL).

3. Results and discussion

3.1. Effect of mechanically activated milling

Fig. 1 shows the SEM images of two starting powders (Al_2O_3 and $BaCO_3$) and ball-milled powders. It is clearly seen that the particle sizes of the $BaCO_3$ powder are reduced during the high-energy ball milling. The initial shape of the $BaCO_3$ particles could not be found anymore after milling. As for Al_2O_3, it seems that no evident particle refinement occurs after 9 h milling (Fig. 1(c)). On the contrary, when the powders were ball-milled for 72 h, as shown in Fig. 1(d), their particle sizes look like larger than those of the initial Al_2O_3 powder. This is likely to be due to the agglomeration of particles during the milling.

The X-ray diffraction patterns of the ball-milled powders with different milling times are shown in Fig. 2. All the XRD profiles of the ball-milled powders are similar to that of the mixture of two starting powders (*i.e.*, milling time of 0 h in Fig. 2(a)). The patterns consisted only of Al_2O_3 and $BaCO_3$ phases and no new phase was detected even after milling for 72 h. This indicates that the ball-milling process is not able to directly result in the reaction between Al_2O_3 and $BaCO_3$ as well as the formation of Ba-β-Al_2O_3 phase. However, the broadening of peaks (especially peaks of $BaCO_3$) occurred. For example, the half-value width of the strongest peak of $BaCO_3$ at $2\theta = 24.5^\circ$ became larger, suggesting the refinement of $BaCO_3$ crystalline sizes due to deformation during the ball milling. Moreover, a hump at $2\theta = 33^\circ$ (corresponding to $BaCO_3$) was also

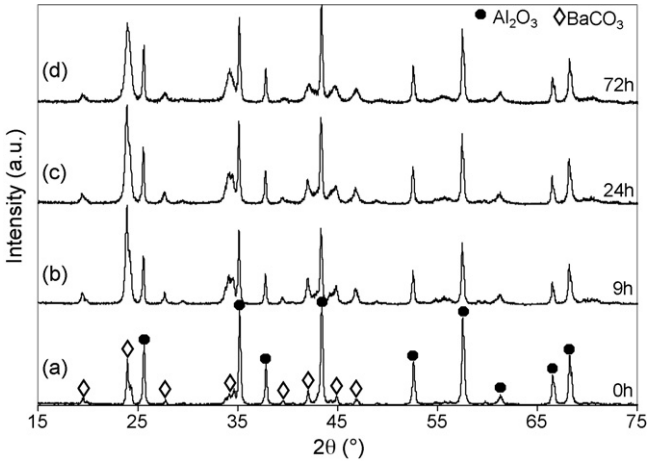

Fig. 2. X-ray diffraction patterns of ball-milled powders with different milling times.

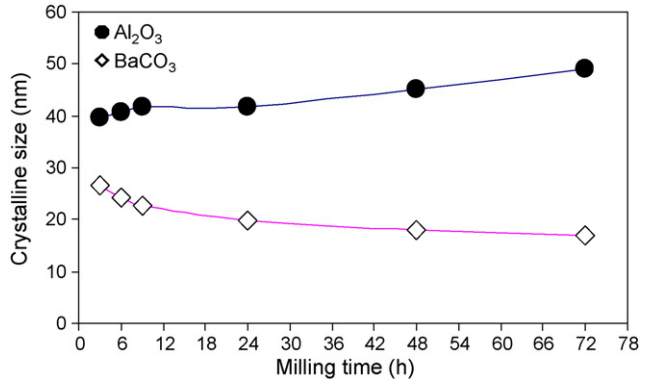

Fig. 3. Crystalline sizes of alumina and barium carbonate powders as a function of milling time.

found with increasing milling time, which implies an increase of amorphization degree.

The crystalline sizes of both Al_2O_3 and $BaCO_3$ were determined from the XRD results by means of the Scherrer formula, and the results are shown in Fig. 3. The longer the milling time, the smaller the crystalline size of the $BaCO_3$ powder, as expected. For Al_2O_3 powder, however, the crystalline size increases with the milling time. The variations of the crystalline sizes are consistent with those of the particle sizes of the Al_2O_3 and $BaCO_3$ powders (Fig. 1). These results show that the milling process cannot refine the Al_2O_3 particles anymore, presumably due to their small initial particle sizes (average size: 0.17 μm). The milling process only increases the lattice strain of the Al_2O_3 powder, not resulting in a further refinement in both crystalline size and particle size. This phenomenon was also found on high-energy milling of $Bi_5Nb_3O_{15}$ and Bi_3NbO_7 powders [18].

In order to obtain Ba-β-Al_2O_3 compound, all milled powder samples including 0-h-milled powder (without milling) were heat-treated at 1500 °C for 2 h. The XRD results of the heat-treated samples are shown in Fig. 4. As a reference, a standard XRD pattern of the Ba-β-Al_2O_3 phase was also included in the figure. For the raw mixture without milling, the heat treatment at 1500 °C

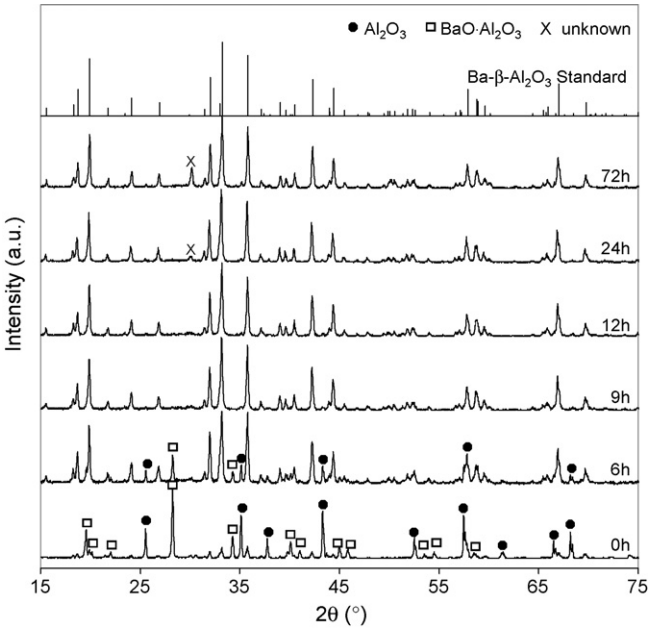

Fig. 4. XRD patterns of ball-milled powders with different milling times after heat treatment at 1500 °C for 2 h.

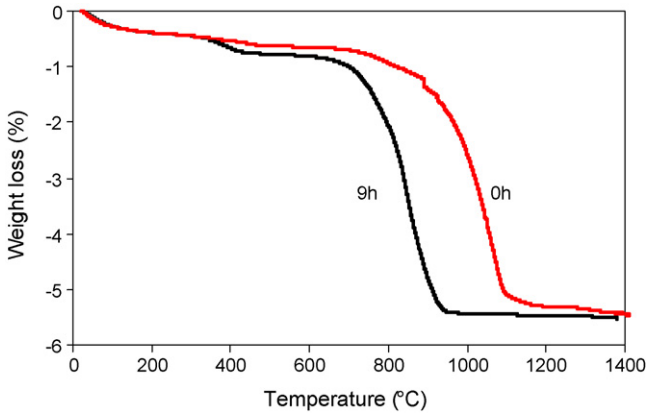

Fig. 5. Weight loss curves of 0-h- and 9-h-milled powders during heating in air. Heating rate: 10 °C/min.

resulted in formation of $BaO{\cdot}Al_2O_3$ and Ba-β-Al_2O_3 with unreacted Al_2O_3 remaining. However, the intensity of the Ba-β-Al_2O_3 peaks was very small. As the milling time increased, the intensity of the Al_2O_3 and $BaO{\cdot}Al_2O_3$ peaks gradually decreased, while that of the Ba-β-Al_2O_3 peaks increased. These results reveal that the milling process does have a significant effect on the formation of Ba-β-Al_2O_3 compound. The high-energy ball milling promotes the reactions between Al_2O_3 and $BaCO_3$ (or BaO formed by decomposition of $BaCO_3$, to be discussed later) as well as between Al_2O_3 and $BaO{\cdot}Al_2O_3$. When milling for 9–12 h, the XRD patterns corresponded to Ba-β-Al_2O_3 as a dominant phase and a trace of Al_2O_3. But for milling longer than 12 h, there was an unknown peak at $2\theta = 30.22°$. This peak might be associated with zirconia phase that comes from the vial or milling balls. From the above results, it can be concluded that it is possible to synthesize almost monophasic Ba-β-Al_2O_3 through mechanically activated milling of Al_2O_3–$BaCO_3$ powder mixture at 200 rpm for 9–12 h, followed by heat treatment at 1500 °C for 2 h.

3.2. TG and DSC analyses

Fig. 5 shows the weight changes of the 0-h- and 9-h-milled samples during heating in air. In both cases, the final weight losses during the measurements were about 5 wt% with respect to the initial sample weights. A slight weight loss occurred in the initial heating period up to ~700 °C, followed by a rapid weight reduction with increasing the temperature above ~700 °C. The former may be associated with the dehydration of some hydrates, while the latter is attributed to the decomposition of $BaCO_3$ through the following reaction:

$$BaCO_3 \rightarrow BaO + CO_2 \quad (g) \qquad (1)$$

It is easily found from Fig. 5 that the 9-h-milled sample corresponds to a decomposition temperature range, 700–900 °C, which is ~200 °C lower than that of the non-milled sample (0 h). This indicates that the mechanically activated milling has a significant effect on decomposition of $BaCO_3$. The ball milling causes an evident decrease in the decomposition temperature of $BaCO_3$. This is obviously related to the refinement of the $BaCO_3$ particles, an introduction of lattice strain, and an increase in reactivity in the ball-milled powder.

It is well known that endothermic decomposition with the liberation of carbon dioxide is the most characteristic property of carbonates [19]. To further clarify the decomposition behavior of $BaCO_3$ and its reaction with Al_2O_3 during heating, the DSC analysis of the milled powder has been carried out and the results are illustrated in Fig. 6. All three curves, corresponding to 0-h-, 9-h-

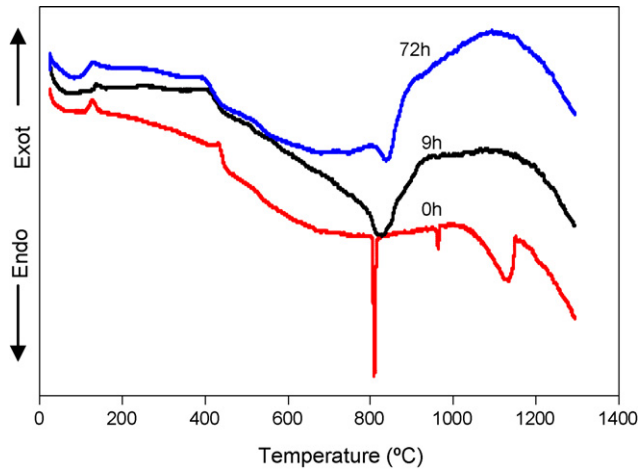

Fig. 6. DSC curves of 0-h-, 9-h-, and 72-h-milled powder samples.

, and 72-h-milled powders, show two small exothermal peaks at around 130 °C and 400 °C, respectively. The occurrence of these exothermal peaks is probably associated with the dehydration process, which is in agreement with the small weight changes in the TG results shown in Fig. 5. For the non-milled sample, three endothermic peaks, centered at 810 °C, 964 °C, and 1134 °C, respectively, were identified. The two sharp peaks at 810 °C and 964 °C are believed to be due to polymorphic transformations of $BaCO_3$. The strong endothermic peak at 810 °C corresponds to the orthorhombic–hexagonal transformation, whereas the peak at 964 °C is concerned with the hexagonal-cubic transformation [19–21]. In comparison with Figs. 5 and 6, it is believed that the third endothermic peak with a broad temperature range, started at ~1000 °C and centered at 1134 °C, is attributed to the decomposition of $BaCO_3$. Nevertheless, a significant weight loss due to the decomposition of $BaCO_3$ occurs from a quite lower temperature, for instance, ~700 °C (Fig. 5) for the milled powder. This fact suggests that the decomposition of $BaCO_3$ takes place simultaneously during the polymorphic transformations of $BaCO_3$.

Concerning the ball-milled powders, as described before, due to the refinement of particles, the decomposition of $BaCO_3$ shifted to lower temperatures. From the TG results shown in Fig. 5, it is reasonable to consider that the endothermic peaks centered at 825 °C and 838 °C in Fig. 6 mainly correspond to the decomposition of $BaCO_3$ for 9-h- and 72-h-milled powders, respectively.

3.3. Phase and microstructure evolution during heat treatment

The XRD patterns illustrating the phase transformation of a 9-h-milled powder sample during the heat treatment at different temperatures ranging from 600 °C to 1500 °C are shown in Fig. 7. Variations of the phases and their qualitative composition with heat-treatment temperature are summarized in Table 1. Until 600 °C, the XRD pattern was almost the same as that of the as-ball-milled powder (Fig. 2(b)), *i.e.*, only the peaks of Al_2O_3 and $BaCO_3$ being detected. The degree of crystallinity of the ball-milled powder (especially $BaCO_3$) was improved with increasing the heat-treatment temperature.

When the heat treatment was performed at 800 °C, a small peak corresponding to $BaO{\cdot}Al_2O_3$ was detected at $2\theta = 28.32°$ (Fig. 7). Since BaO has already started to form at ~700 °C (Fig. 5) according to Eq. (1), it is reasonable to consider that the formation of $BaO{\cdot}Al_2O_3$ arises from the decomposition of $BaCO_3$ and subsequent reaction with Al_2O_3 by

$$BaO + Al_2O_3 \rightarrow BaO{\cdot}Al_2O_3 \quad (2)$$

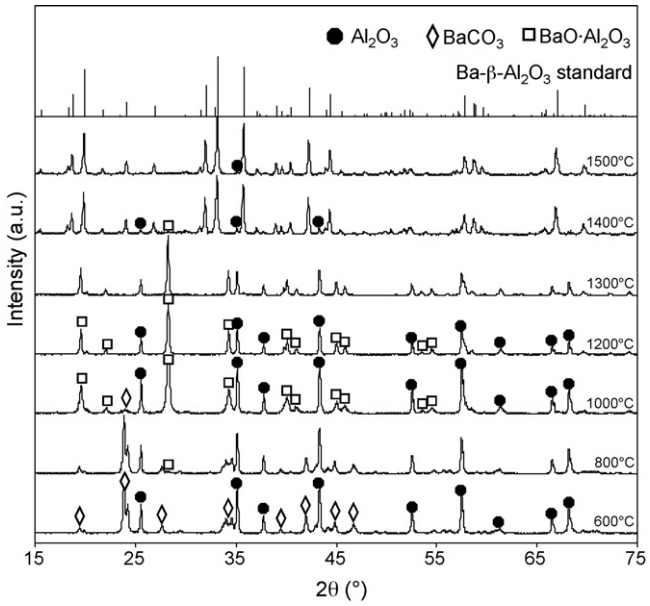

Fig. 7. XRD patterns showing the phase change of 9-h-milled powder during heat treatment at different temperatures.

At 1000 °C, the intensity of the $BaCO_3$ peaks was greatly reduced and only trace amount of $BaCO_3$ remained. As a result, $BaO{\cdot}Al_2O_3$ became one of the main phases. These facts gave an evidence of the decomposition of $BaCO_3$ and formation of $BaO{\cdot}Al_2O_3$, which are consistent with the TG and DSC results (Figs. 5 and 6).

At 1200 °C, the $BaCO_3$ peaks completely disappeared and, thus, only two phases, Al_2O_3 and $BaO{\cdot}Al_2O_3$, were present. These two phases were stable up to 1300 °C. At 1400 °C, however, the dominant phase was Ba-β-Al_2O_3 ($Ba_{0.75}Al_{11}O_{17.25}$ or $BaO{\cdot}7.3Al_2O_3$) with weak intensity of Al_2O_3 and a trace of $BaO{\cdot}Al_2O_3$ remaining. This suggests that $BaO{\cdot}Al_2O_3$ is an intermediate phase in synthesizing Ba-β-Al_2O_3 and Ba-β-Al_2O_3 is formed through reaction between $BaO{\cdot}Al_2O_3$ and Al_2O_3 by following formula:

$$BaO{\cdot}Al_2O_3 + 6.3Al_2O_3 \rightarrow BaO{\cdot}7.3Al_2O_3 \quad (3)$$

This is in good agreement with our previous research [4,5].

At 1500 °C, as a result of a further reaction of remnant $BaO{\cdot}Al_2O_3$ with Al_2O_3 (Eq. (3)), almost single phase of Ba-β-Al_2O_3 was obtained with trace of Al_2O_3. Moreover, during the heat treatment, the intensity of Al_2O_3 peaks gradually decreased with increasing the heat-treatment temperature. For example, at 1000 °C, Al_2O_3 was one of the dominant phases, whereas at 1500 °C its intensity became extremely low.

Table 1
Variations of phases and their qualitative composition with heat-treatment temperature.

Temperature (°C)	Phases[a]			
	Al_2O_3	$BaCO_3$	$BaO{\cdot}Al_2O_3$	Ba-β-Al_2O_3
20[b]	s	s	–	–
400	s	s	–	–
600	s	s	–	–
800	s	s	t	–
1000	s	t	s	–
1200	s	–	s	–
1300	s	–	s	–
1400	w	–	t	s
1500	t	–	–	s

[a] s: strong, w: weak, t: trace, –: none.
[b] 9-h-milled powder (without any heat treatment).

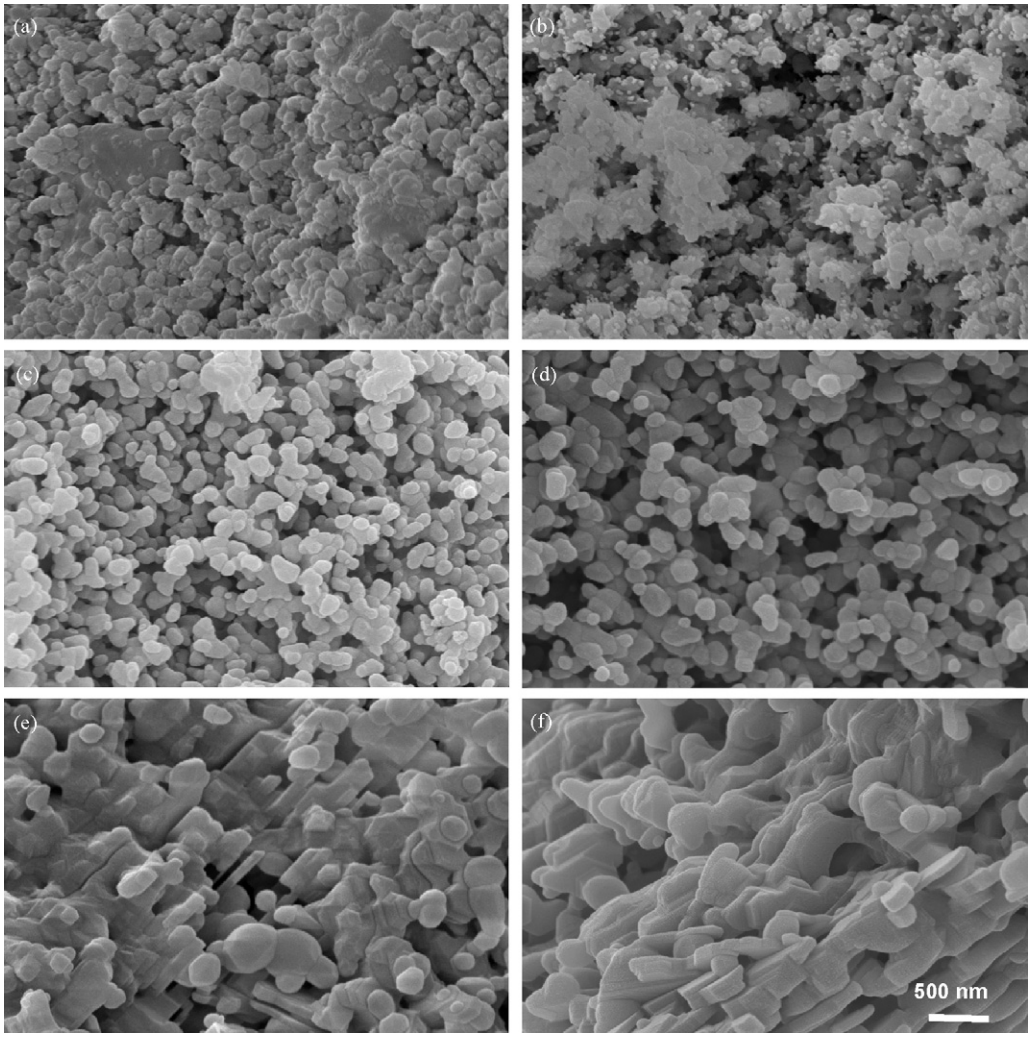

Fig. 8. Morphological evolution of 9-h-milled powder during heat treatment at different temperatures: (a) 800 °C, (b) 1000 °C, (c) 1200 °C, (d) 1300 °C, (e) 1400 °C, and (f) 1500 °C.

Fig. 8 shows the morphological evolution of the 9-h-milled powder during the heat treatment. No evident morphological change of particles was observed after heat treatment below 800 °C. At 800 °C, it seems that there are some agglomerated regions in the SEM image (Fig. 8(a)), in comparison with the as-ball-milled powder shown in Fig. 1(c). These agglomerated regions may arise from the decomposition of $BaCO_3$ phase, as has been confirmed by TG (Fig. 5), DSC (Fig. 6), and XRD (Fig. 7) analyses. Even though the $BaO{\cdot}Al_2O_3$ phase has started to form at 800 °C from the XRD results, it is difficult to find its existence from the SEM image, presumably due to its small size and amount. At 1000 °C (Fig. 8(b)), however, a large number of nanosized particles (20–40 nm) are generated and distributed on the surfaces of some larger Al_2O_3 and $BaCO_3$ particles homogeneously. These small particles result from $BaO{\cdot}Al_2O_3$ phase formed through the reaction between Al_2O_3 and BaO. Also, it appears that there are some pores with a size level similar to the $BaO{\cdot}Al_2O_3$ particles, which may originate from the evaporation of CO_2 gas due to the decomposition of $BaCO_3$.

As the temperature increased, $BaCO_3$ was gradually decomposed and finally disappeared completely at 1200 °C. Concurrent with the decomposition of $BaCO_3$, the $BaO{\cdot}Al_2O_3$ particles grew and this process continued until 1300 °C. In the temperature range of 1200–1300 °C (Fig. 8(c) and (d)), the particle sizes of Al_2O_3 and $BaO{\cdot}Al_2O_3$ were around 100–200 nm, much finer than those (500–1000 nm) reported by Machida et al. [10]. At 1400 °C (Fig. 8(e)), the microstructure revealed an elongated morphology of particles in which some spherical particles with a submicron order were distributed homogeneously. The elongated particles corresponds to Ba-β-Al_2O_3 that constitutes a dominant phase, while the spherical particles consist of Al_2O_3 and/or $BaO{\cdot}Al_2O_3$ as minor phases. At 1500 °C (Fig. 8(f)), the microstructure is characterized by almost single phase of Ba-β-Al_2O_3 with a trace amount of small spherical Al_2O_3 particles remaining.

From the above microstructural observations, it was noted that the Ba-β-Al_2O_3 compound, obtained from Al_2O_3–$BaCO_3$ powder mixture, exhibited an elongated morphology. This morphological feature is similar to that of Ba-β-Al_2O_3 phase, formed through reaction between Al_2O_3 and $BaZrO_3$ [22–24]. The elongated morphology of Ba-β-Al_2O_3 phase is believed to be due to preferred orientational growth through directional diffusion and mass transport of Ba along the basal plane [24]. These elongated Ba-β-Al_2O_3 particles can be used as a reinforcement [4] to enhance the fracture toughness of ceramic matrix composites through crack deflection and/or crack bridging, just like the functions of whiskers and fibers with large aspect ratios.

On the basis of the phase and microstructure evolution mentioned above, a schematic illustration on the reaction sequence and formation mechanism of the Ba-β-Al_2O_3 phase during heat treatment is given in Fig. 9. When a ball-milled Al_2O_3–$BaCO_3$ powder mixture is heat-treated below 600 °C, no phase change can be

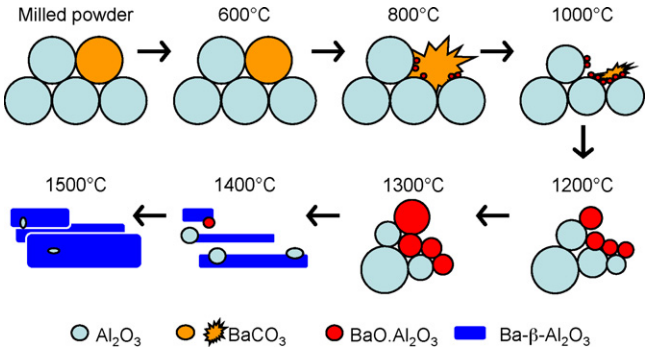

Fig. 9. A schematic illustration showing the formation of elongated Ba-β-Al_2O_3 during heat treatment.

confirmed. From ~700 °C, $BaCO_3$ starts to decompose. In a temperature range of 700–1100 °C, $BaCO_3$ is rapidly decomposed into BaO and then reacts with Al_2O_3 to form nanosized $BaO{\cdot}Al_2O_3$ particles. At 1000 °C, $BaO{\cdot}Al_2O_3$ becomes one of the dominant phases with Al_2O_3 and minor $BaCO_3$, and $BaCO_3$ is completely disappeared at 1200–1300 °C. With increasing the temperature, $BaO{\cdot}Al_2O_3$ gradually grows and further reacts with Al_2O_3 to change into Ba-β-Al_2O_3 above 1400 °C. At 1500 °C, almost monophasic Ba-β-Al_2O_3 is synthesized with a trace amount of Al_2O_3 particles remaining. Consequently, the formation of Ba-β-Al_2O_3 phase can be roughly divided into three stages: (i) decomposition of $BaCO_3$, (ii) formation and growth of $BaO{\cdot}Al_2O_3$ particles, and (iii) formation of Ba-β-Al_2O_3 phase with an elongated morphology.

4. Conclusions

Mechanically activated milling cannot result in direct formation of Ba-β-Al_2O_3 from a powder mixture of Al_2O_3 and $BaCO_3$. However, it has significant effects on lowering decomposition temperature of $BaCO_3$ and promoting its subsequent reactions with Al_2O_3. Almost monophasic Ba-β-Al_2O_3 powder can be synthesized by high-energy planetary ball milling at 200 rpm for 9–12 h, followed by solid-state reaction at 1500 °C for 2 h. Based on the results of TG, DSC, XRD, and SEM studies, the most probable reaction sequences leading to the formation of Ba-β-Al_2O_3 were, (i) decomposition of $BaCO_3$ from ~700 °C, (ii) formation and growth of spherical $BaO{\cdot}Al_2O_3$ particles, and (iii) formation of Ba-β-Al_2O_3 phase with an elongated morphology at 1500 °C. $BaO{\cdot}Al_2O_3$ is proved to be an intermediate phase in the process of forming Ba-β-Al_2O_3.

Acknowledgment

The first author (SN) gratefully acknowledges the Ministry of Education, Culture, Sports, Science and Technology of Japan, for providing financial support during the study and this research at Tohoku University.

References

[1] M. Mohapatra, D.M. Pattanaik, S. Anand, R.P. Das, Ceram. Int. 33 (4) (2007) 531–535.
[2] G. Groppi, C. Cristiani, P. Forzatti, M. Belloto, J. Mater. Sci. 29 (1994) 3441–3450.
[3] G. He, T. Goto, T. Narushima, Y. Iguchi, Solid State Ionics 121 (1999) 313–319.
[4] Z. Chen, K.K. Chawla, M. Koopman, Mater. Sci. Eng. A 367 (2004) 24–32.
[5] Z. Chen, T. Okazawa, K. Ikeda, Ceram. Trans. 192 (2006) 11–21.
[6] S. Kimura, E. Bannai, I. Shindo, Mater. Res. Bull. 17 (1982) 209–215.
[7] N. Iyi, Z. Inoue, S. Takekawa, S. Kimura, J. Solid State Chem. 52 (1) (1984) 66–72.
[8] N. Iyi, S. Takekawa, S. Kimura, J. Solid State Chem. 59 (2) (1985) 250–253.
[9] N. Iyi, S. Takekawa, S. Kimura, J. Solid State Chem. 83 (1) (1989) 8–19.
[10] M. Machida, K. Eguchi, H. Arai, J. Am. Ceram. Soc. 71 (12) (1988) 1142–1147.
[11] J.C. Debsikdar, O.S. Sowemimo, J. Mater. Sci. Lett. 11 (10) (1992) 637–638.
[12] J.C. Debsikdar, J. Mater. Sci. 24 (1989) 3565–3572.
[13] T.J. Davies, H.G. Emblem, M. Biedermann, Q.G. Chen, W.A. Al-Douri, J. Mater. Sci. Lett. 17 (1998) 1845–1847.
[14] D. Mishra, S. Anand, R.K. Panda, R.P. Das, Mater. Lett. 56 (2002) 873–879.
[15] M. Uzawa, M. Kayawa, Y. Syono, Mater. Lett. 17 (1993) 187–189.
[16] L.B. Kong, J. Ma, W. Zhu, O.K. Tan, J. Alloys Compd. 322 (2001) 290–297.
[17] B. Djuricic, S. Pickering, D. McGarry, J. Mater. Sci. 34 (1999) 2685–2694.
[18] D. Zhou, H. Wang, X. Yao, L.X. Pang, H.F. Zhou, J. Am. Ceram. Soc. 91 (1) (2008) 139–143.
[19] R.C. Mackenzie, Differential Thermal Analysis, Academic Press, London, 1979, p. 306.
[20] M.I. Zaki, G.A.M. Hussien, R.B. Fahim, J. Mater. Sci. Lett. 4 (1985) 517–522.
[21] I. Arvanitidis, D. Sichen, S. Seetharaman, Metal. Mater. Trans. B 27B (3) (1996) 410–416.
[22] Z. Chen, S. Duncan, K.K. Chawla, M. Koopman, G.M. Janowski, Mater. Charact. 48 (2002) 305–314.
[23] Z. Chen, R. Kulkarni, K.K. Chawla, M. Koopman, K. Ikeda, Mater. Sci. Forum 475–479 (2005) 1301–1304.
[24] Z. Chen, T. Tamachi, R. Kulkarni, K.K. Chawla, M. Koopman, J. Eur. Ceram. Soc. 28 (2008) 1149–1160.